

LinearAlifold: Linear-Time Consensus Structure Prediction for RNA Alignments

Liang Zhang,¹ Sizhen Li,¹ He Zhang,² David H. Mathews,^{3,4,5} Liang Huang^{1*}

¹School of EECS, Oregon State University, Corvallis, OR 97330, USA

²Baidu Research USA, Sunnyvale, CA 94089, USA

³Dept. of Biochemistry & Biophysics, ⁴Center for RNA Biology, and

⁵Dept. of Biostatistics & Computational Biology,
University of Rochester Medical Center, Rochester, NY 14642, USA

*To whom correspondence should be addressed.

Predicting the consensus structure of a set of aligned RNA homologs is a convenient method to find conserved structures in an RNA genome, which has applications in SARS-CoV-2 diagnostics and therapeutics. However, the state-of-the-art algorithm for this task, RNAalifold, is prohibitively slow for long sequences, due to a cubic scaling with the sequence length, and even slower when analyzing many such sequences, due to a superlinear scaling with the number of homologs, taking 4 days on 200 SARS-CoV variants. We present LinearAlifold, an efficient algorithm for folding aligned RNA homologs that scales linearly with *both* the sequence length and the number of sequences, based on our recent work LinearFold that folds a single RNA in linear time. Our work is orders of magnitude faster than RNAalifold (e.g., 0.5 hours on the above 200 sequences, or 316× speedup) and achieves comparable accuracies compared to a database of known structures. More interestingly, LinearAlifold’s prediction on SARS-CoV-2 correlates well with experimentally determined structures, outperforming RNAalifold. Finally, LinearAlifold supports three modes: minimum free energy (MFE), partition function, and stochastic sampling, each of which takes under an hour for hundreds of SARS-CoV variants, while only the MFE mode of RNAalifold works for them, taking days or weeks.

Introduction

Ribonucleic acids (RNA) are involved in many cellular processes [12, 11, 3], and most of RNA secondary structures are highly conserved across evolution to maintain their functionalities in spite of changes to the sequence [25, 5, 26]. Thus, predicting the *consensus structure* for a set of aligned RNA homologs is more accurate than predicting the structure for a single sequence and it is useful for identifying conserved regions, which can be used for diagnostics and therapeutics. For this task, RNAalifold [15, 4] is a widely used tool to predict consensus structures for aligned RNA homologs that considers both thermodynamic stability and sequence covariation. However, its cubic runtime (against sequence length n) makes it difficult to be applied to long sequences such as SARS-CoV-2 genomes ($n \simeq 30,000nt$). Furthermore, it also scales superlinearly in practice with the number of sequences (k), which worsens its runtime when considering many long homologs. For example, to combat the COVID-19 pandemic, it is often helpful to include hundreds of SARS-CoV-2 and SARS-related genomes to account for as much sequence variation as possible, as new variants emerge rapidly, but this task takes prohibitively long for RNAalifold (4 days for $k = 200$ genomes, and weeks for $k = 400$). On the other hand, beyond predicting minimum free energy (MFE) consensus structures, it is also useful to calculate the *consensus partition function* and *consensus base-pairing probabilities*, which are widely used in many downstream tasks such as maximum expected accuracy (MEA) folding [20, 10, 24] and stochastic sampling from the ensemble [9, 30]. For example, LinearTurboFold [22] uses stochastic sampling to identify conserved and accessible regions for diagnostics and therapeutics in SARS-CoV-2 genomes. However, RNAalifold’s partition function mode is even slower than its MFE mode (often by 10× or more), and both its partition function and stochastic sampling modes fail to run on SARS-CoV-2 variants (for any $k > 1$) due to overflow.

To alleviate this slow runtime, one can use local folding to predict consensus structures in linear time. However, such a heuristic rules out non-local interactions. Those interactions, especially the end-to-end ones, are known to be prevalent in most RNAs [8, 21]. In particular, the base pairs between the 5’ and 3’ untranslated regions (UTRs) of SARS-CoV-2, across $\sim 30,000$ nucleotides, are found by both purely experimental methods [33] and by purely computational ones [22]. How can we speed up consensus structure

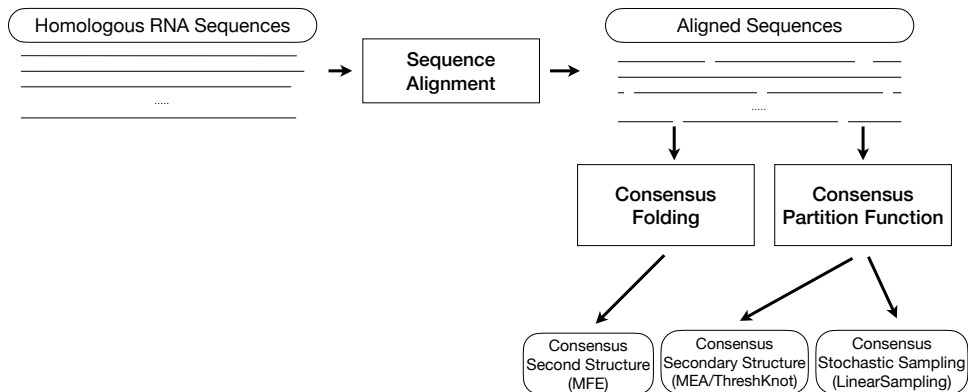


Figure 1: Overview of LinearAlifold. LinearAlifold takes aligned homologous sequences as input to predict consensus structures, consensus partition function, and consensus base-pairing probabilities, which are widely used in downstream tasks such as Maximum Expected Accuracy (MEA) [20, 10, 24] folding, ThreshKnot [32] folding, and stochastic sampling from the ensemble [9, 30].

prediction without sacrificing long-distance pairs?

Here we report LinearAlifold, an efficient algorithm for consensus structure prediction that scales *linearly* with both the sequence length (n) and the number of aligned sequences (k) without any constraints on pair distance, building upon on our recent work LinearFold [17] and LinearPartition [31] for single sequence folding (Fig. 1). Being orders of magnitude faster than RNAalifold, our work can fold hundreds of full-length coronavirus genomes under an hour and can recover end-to-end pairs. For example, it takes only 0.5 hours to fold the above-mentioned $k = 200$ SARS-CoV sequences, compared to 4 days by RNAalifold (316 \times speedup). Meanwhile, LinearAlifold is comparable to RNAalifold in structure prediction accuracy compared to a database of known structures of homologous sequences [29]. More importantly, LinearAlifold’s predictions on hundreds of SARS-CoV genomes (under an hour) correlate better with the experimentally guided structures [18, 33] than RNAalifold’s (over a week) (Figs. 4–5). In addition to MFE folding, LinearAlifold also supports partition function, base-pairing probabilities, ensemble-based structure prediction methods MEA and Threshknot, and stochastic sampling, all of which take under an hour on hundreds of SARS-CoV variants. Following LinearTurboFold’s method for targeting regions that are sequence-level conserved and structurally accessible, we used LinearSampling [30] algorithm to identify these regions. These conserved and accessible regions are potential targets for small molecule drugs [14], anti-

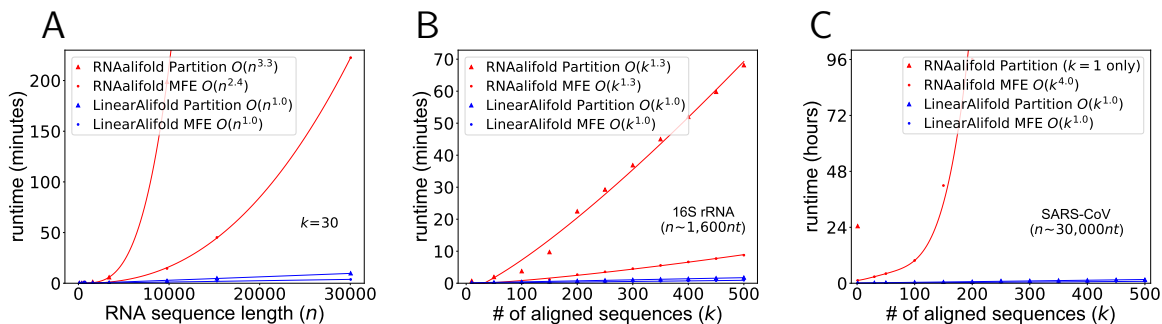


Figure 2: Runtime comparisons between RNAalifold and LinearAlifold ($b = 100$). **A**: runtime comparison against sequence length (n) on multiple sequence alignment (MSA) at number of aligned sequences (k) = 30. **B**: runtime comparison against k on a set of 16S rRNA family MSAs ($n \simeq 1,600nt$). **C**: runtime comparison against k on a set of SARS-CoV-2 and SARS-related genome MSAs ($n \simeq 30,000nt$). Because RNAalifold fails to run on SARS-CoV MSAs for $k > 1$, we only show $k = 1$ result for RNAalifold in the partition function mode here. RNAalifold cannot run on MSAs with $n > 32,768nt$ due to a data structure limit. Thus, all of our SARS-CoV MSAs’ sequence lengths have to be within the limits. LinearAlifold does not have this limit.

sense oligonucleotides (ASOs) [28], small interfering RNA (siRNA) [27], CRISPR-Cas13 guide RNA (gRNA) [1], and reverse transcription polymerase chain reaction (RT-PCR) primes [6].

Results

RNAalifold and LinearAlifold take a multiple-sequence alignment (MSA) as input (Fig. 1) and outputs an MFE consensus structure or a consensus partition function. The folding scoring model in the two systems is a ‘consensus model’ guided by folding thermodynamics and sequence covariation [15, 4]. We employed the beam pruning heuristic to reduce the complexity from cubic runtime (against n) to linear time, inspired by LinearFold [17]. The basic idea of the heuristic algorithm is, at each step j , we only keep the b top-scoring states and prune the other ones, which are less likely to be part of the optimal final structure. This approximate search algorithm helps reduce the time complexity from $O(kn^3)$ to $O(knb^2)$. In the MFE mode, we further reduced the time complexity to $O(knb \log b)$ following the k -best parsing idea from Huang and Chiang [16]. We set the beam size by default 100, following LinearFold and LinearPartition. Thus, we reduced the time complexity from $O(kn^3)$ (RNAalifold) to $O(kn)$ (LinearAlifold).

Scalability

To demonstrate the effectiveness of our work, we prepared a set of RNA sequences that contains 8 families ($n \simeq 1,600nt$ or less) from RNAStralign [29], 23s rRNA ($n \simeq 3,300nt$) from the Comparative RNA Web (CRW) site [7], and long sequences (from $\sim 9,800nt$ to $\sim 30,000nt$) from three viruses ¹ from NCBI² and GISAID³. We used MAFFT [19] to align the input sequences.

Fig. 2 compares the empirical runtime of RNAalifold and LinearAlifold. As shown in Fig. 2A, for a given k , it is clear that LinearAlifold scales linearly with sequence length n and is substantially faster than RNAalifold under either the MFE or the partition function modes. RNAalifold’s empirical runtime scales $n^{2.4}$ in the MFE mode and $n^{3.3}$ in the partition function mode. Under the MFE mode, LinearAlifold takes only 3.7 minutes (224 seconds) on the SARS-CoV family ($n \simeq 30,000nt$, $k = 30$), while RNAalifold takes 3.7 hours (60× speedup). Furthermore, RNAalifold cannot scale to $n > 14,000nt$ for $k = 30$ under the partition function mode. Thus, we tested on the HIV family ($\simeq 9,800nt$) on which both RNAalifold and LinearAlifold can run. LinearAlifold and RNAalifold require 2.4 minutes (142 seconds) and 3.3 hours (84× speedup, $k = 30$), respectively. We also tested the empirical runtime against the number of homologs (k) using 16S rRNA ($n \simeq 1,600nt$) and SARS-CoV ($n \simeq 30,000nt$) (Fig. 2B–C). On 16S, our work scales linearly with k while RNAalifold scales $k^{1.2}$ in time. More interestingly, on SARS-CoV, our work is still linear against k in both the MFE and the partition modes, but RNAalifold’s empirical runtime scales k^4 in the MFE mode. For $k = 200$, RNAalifold already requires 4 days on SARS-CoV, and it takes more than one week time for $k \geq 300$ in the MFE mode. In addition, RNAalifold cannot run for $k > 1$ on SARS-CoV in the partition function mode due to overflow.

The space complexity of our work is $O(n^2 + kn + bn)$, where the first, second, and third parts correspond to storing the covariance scores (see Methods), the input MSA, and the dynamic programming items, respectively. RNAalifold requires the same space complexity to keep the covariance scores and the input, but $O(n^2)$ for items. So the space complexity of RNAalifold is $O(n^2 + kn + n^2)$. In practice, on SARS-CoV with

¹HIV (human immunodeficiency virus, $n \simeq 9,800nt$), RSV (Respiratory syncytial virus, $n \simeq 15,000nt$), and SARS-CoV ($n \simeq 30,000nt$) genomes

²www.ncbi.nlm.nih.gov

³www.gisaid.org

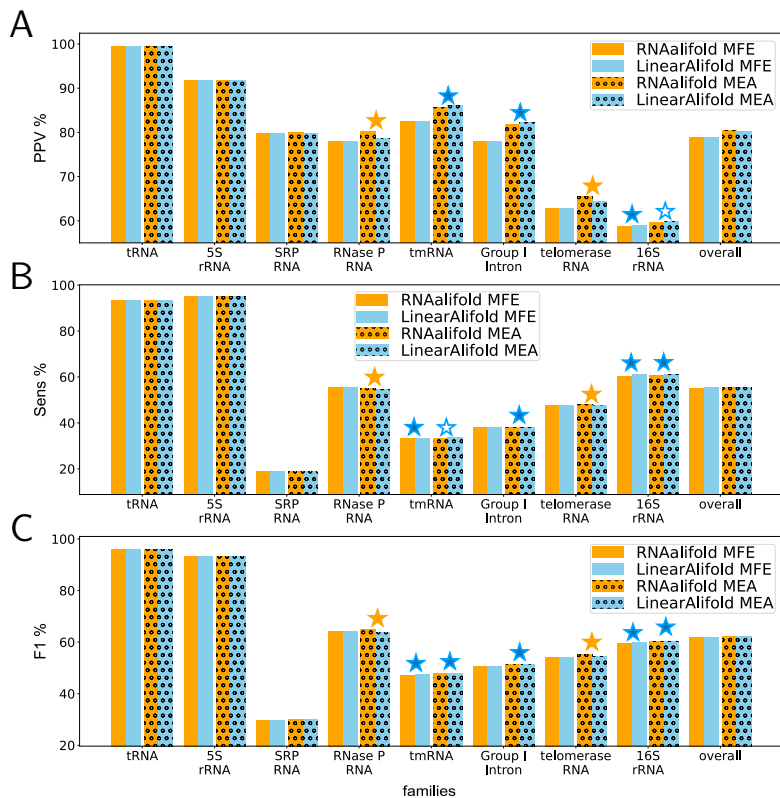


Figure 3: Accuracy comparisons between RNAalifold and LinearAlifold on $k = 30$ MSAs for each family. The Minimum Free Energy (MFE) and The Maximum Expected Accuracy (MEA, $\gamma = 1.0$, RNAalifold default setting) results are reported. **A**: positive predictive value (PPV; a.k.a. precision) of the structure prediction. **B**: sensitivity (a.k.a. recall) of the structure prediction. **C**: F1 accuracy scores of the structure prediction. Statistical significance (two-sided) is marked as LinearAlifold is significantly better: ‘☆’: $0.01 \leq p < 0.05$, ‘★’: $p < 0.01$), or RNAalifold is significantly better: ‘☆’: $0.01 \leq p < 0.05$, ‘★’: $p < 0.01$).

$k = 30$, LinearAlifold requires 7.9 GB in the MFE mode and 9.3 GB memory in the partition function mode, while RNAalifold requires 6.3 GB in the MFE mode, and it cannot scale to SARS-CoV in the partition function mode (see Fig. S1A). As shown in Fig. S1B, both LinearAlifold and RNAalifold space complexities scale linearly with k , and the memory usage of LinearAlifold keeps under 9 GB in the MFE mode and under 11 GB in the partition mode for any $k \leq 500$.

Accuracy

Using the eight families from RNAStralign, which have well-determined secondary structures, we compared the accuracies of secondary structure prediction (Fig. 3). The input RNA sequences of each family were firstly aligned using MAFFT before we run RNAalifold and LinearAlifold on them. LinearAlifold achieves comparable accuracies to RNAalifold

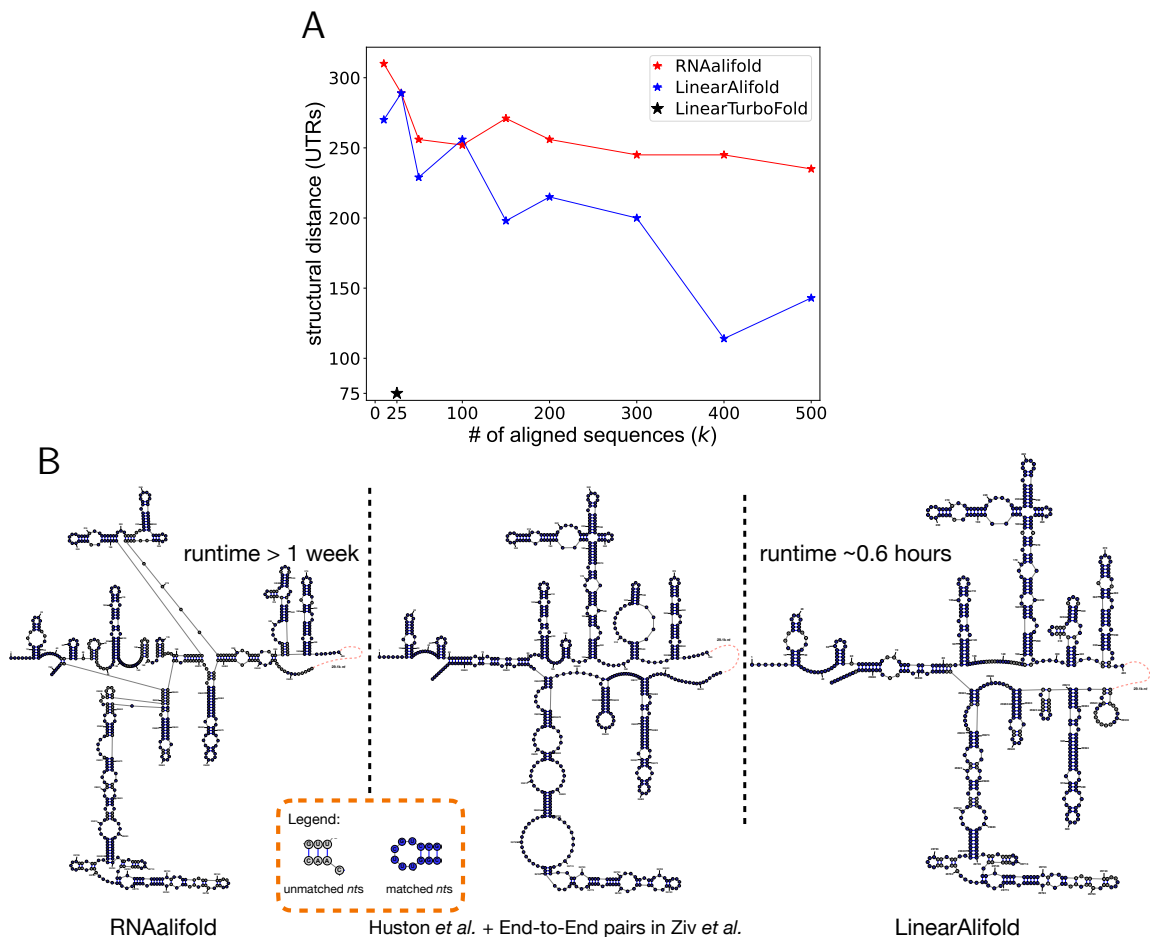


Figure 4: The comparison of the predicted structures (MFE) between RNAalifold and LinearAlifold in the 5' UTR and 3' UTR regions. **A**: structural distance of RNAalifold and LinearAlifold in the 5' UTR and 3' UTR region, benchmarked with a hybrid structure that combines local pairs from Huston *et al.* [18] and end-to-end pairs from Ziv *et al.* [33]. **B**: details of predicted structures. LinearAlifold matches more nucleotides than RNAalifold, benchmarked with the hybrid structure from Huston *et al.* [18] and Ziv *et al.* [33].

in terms of positive predictive value (PPV; a.k.a., precision), sensitivity (a.k.a., recall), and F1 scores. We conducted the significance test [2] and noticed that, compared to RNAalifold, LinearAlifold's PPV, sensitivity, and F1 scores are significantly better on the 16S rRNA family, which contains the longest sequences in the eight families, in both the MFE and the MEA structure predictions.

Consensus Structure Prediction in SARS-CoV-2 and SARS-related Betacoronaviruses

It is known that conserved structures across mutations are critical for viruses to maintain their functions to survive. Thus, these conserved regions could be potential targets for

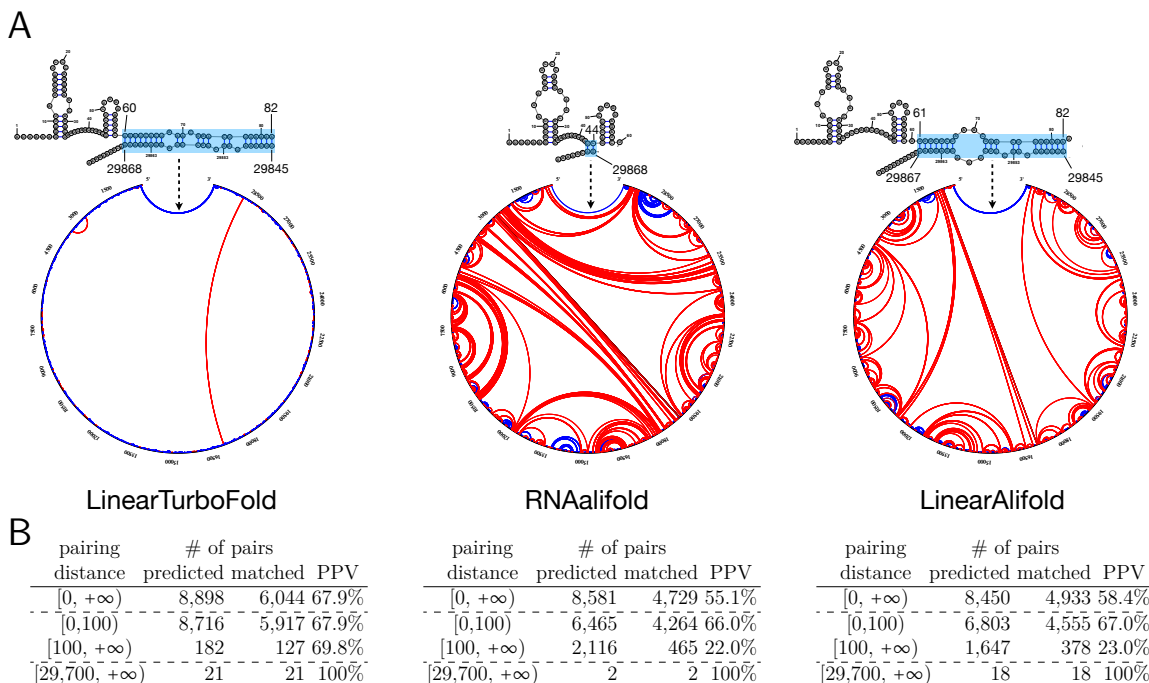


Figure 5: Predicted structures (MFE) of LinearTurboFold, RNAalifold, and LinearAlifold, benchmarked with chimeric reads from Ziv et al. [33]. **A**: correctly predicted base pairs are in blue (true positives), incorrectly predicted pairs in red (false positives). LinearTurboFold and LinearAlifold can find an end-to-end pairing region involving 5' and 3' untranslated regions (UTRs) ($\sim 29,800nt$), which is consistent with a purely experimental work from Ziv et al. [33]. RNAalifold can only find two long-range pairs that match the chimeric reads, but are out of the end-to-end pairing region showed in Ziv et al. [33]. **B**: statistics and predicted accuracies of the three systems against the chimeric reads [33] for different pairing distances.

diagnostics and therapeutics [25, 5, 26]. To model consensus structures for SARS-CoV-2 and SARS-related betacoronaviruses, we first greedily sampled sets of the most diverse sequences with different k 's ranging from 10 to 500 (see Methods for details), and used MAFFT to generate a set of MSAs. Following our work with LinearTurboFold⁴, the ratio of the number of SARS-CoV-2 to the number of SARS-related genomes remains 6 to 4 in all samples.

To evaluate the reliability of LinearAlifold's prediction on SARS-CoV-2, we compared the predicted MFE structure with experimental studies [18, 33] for the well-known 5' and 3' UTR regions. Huston et al. [18] modeled secondary structures guided by the chemical probing data (SHAPE-MaP), but used a local folding method for prediction because the sequence length of SARS-CoV-2 is out of reach of most algorithms. As a result, long-range

⁴LinearTurboFold built a dataset of 25 full-length SARS-CoV genomes consisting of 16 SARS-CoV-2 and 9 SARS-related sequences

interactions were fully abandoned in their prediction, which are critical for regulating the viral transcription and replication pathways [21, 33]. However, LinearAlifold is able to predict global structures without any limitations on sequence length and pairing distance. To overcome this issue, we further involved a purely experimental study [33], which can detect long-range interactions between 5' and 3' UTRs. Therefore, to take into consideration both local and global structures between 5' and 3' UTRs, we built a hybrid structure model by combining Huston et al. [18]'s and Ziv et al. [33]'s predictions (see Methods for details).

We evaluated the structural distances (the number of incorrectly predicted nucleotides) of LinearAlifold's prediction and RNAalifold's prediction from the hybrid structure, respectively (see Methods for details). LinearAlifold's predictions are closer to the experimental studies (with smaller structural distances) than RNAalifold for most values of k , especially for a large k (e.g., $k \geq 400$) (Fig. 4). Moreover, we illustrated the predicted structures from RNAalifold and LinearAlifold with $k = 400$, respectively, and compared them to the hybrid reference structure (Fig. 4B) by marking matched base pairs and unpaired nucleotides in blue. We observed that, compared to the hybrid reference structure, LinearAlifold predicts closer structures than RNAalifold (the number of incorrectly predicted nucleotides reduced from 245 to 114 out of 820 nucleotides).

Given the high reliability on UTR regions, we next explored the complete structure predicted by LinearAlifold along the full-length genome, and compared them with RNAalifold and LinearTurboFold predictions against the chimeric reads from Ziv et al. [33] (Fig. 5) (see Methods for more details). Both LinearAlifold and LinearTurboFold could predict the end-to-end interactions between UTRs, whose structures match with one of the end-to-end interactions listed in Ziv et al. [33, Fig.3], while RNAalifold can only find two end-end pairs, which are not included in the representative end-to-end interactions. In addition, within any range of pairing distance, LinearAlifold always outperforms RNAalifold in terms of PPV.

Studies show that conserved and accessible regions are important for finding potential binding target regions [27, 1, 6, 23]. These regions could be used to design siRNAs, ASOs, CRISPR-Cas13 gRNAs to knockdown viruses, and RT-PCR primers to detect the presence of viruses. To identify sequence-wise conserved and structurally accessible regions in SARS-CoV-2, following LinearTurboFold, we first used a stochastic sampling

algorithm (LinearSampling [31]) to build a representative ensemble of structures by sampling independent secondary structures according to their probabilities in the Boltzmann distribution generated from LinearAlifold, which was built on the whole MSA. Regions of length at least 15 *nt* with at least 50% accessibility, i.e., fully unpaired among a half of samples, are considered to be accessible regions. We then checked whether these accessible regions are also conserved among both SARS-CoV-2 and SARS-related genomes. Compared to the reference sequence (NC_045512.2), regions with at most three mutation sites on the SARS-CoV-2 genomes and at most eight mutation sites on the SARS-related genomes are identified as conserved regions. In total, we detected 40 both conserved and accessible regions (see Tab. S2 for results).

Discussion

Considering the fast mutation rate of RNA viruses such as SARS-CoV-2, accurately identifying conserved regions from homologs is critical to develop mutation-insensitive diagnostics and therapeutics. Consensus folding algorithms, which can take hundreds of aligned homologs to predict consensus structure, are widely-used for this task. However, RNAalifold, the state-of-the-art consensus folding algorithm, scales cubically with the sequence length in runtime, and is prohibitively slow to analyze long RNAs, especially SARS-CoV-2 ($\sim 30,000$ *nt*). For example, RNAalifold takes weeks to predict the consensus structure of 400 aligned SARS-CoV-2 homologs. To alleviate this issue, we present LinearAlifold, an efficient algorithm which scales linearly with both the sequence length (n) and the number of aligned sequences (k). We confirmed that LinearAlifold is orders of magnitude faster compared to RNAalifold. Given an MSA with 200 SARS-CoV-2 homologs, LinearAlifold takes only 0.5 hours and is 316 \times faster than RNAalifold. Regarding the prediction quality compared to RNAalifold, we demonstrated that LinearAlifold achieves comparable accuracies on a benchmark dataset with known structures.

LinearAlifold has three modes: (1) predicting consensus minimum free energy structure (MFE mode); (2) calculating consensus partition function, base pairing probabilities and outputting consensus MEA/ThreshKnot structures (partition function mode); (3) stochastically sampling structures based on consensus partition function (sampling mode). All these three modes can be applied to hundreds of aligned SARS-CoV-2 homologs,

while only the MFE mode of RNAalifold can be applied to such MSAs due to overflow. Comparing the MFE modes of LinearAlifold and RNAalifold on SARS-CoV-2 homologs, LinearAlifold correlates better with the experimentally determined structures. We also demonstrated that the local prediction (with maximum base pair length) of RNAalifold is much worse than LinearAlifold. Using LinearAlifold sampling mode, we are able to identify 40 conserved and accessible regions in SARS-CoV-2 genomes. These regions are potential drug targets for siRNAs, ASOs, CRISPR-Cas13 gRNAs and RT-PCR primers, and are likely to be insensitive to the future mutations.

Finally, LinearAlifold is a general algorithm and can also be applied to analyze other long RNA viruses, such as HIV, WNV (West Nile Virus), and Ebola.

Methods

Details of the LinearAlifold Algorithm

RNAalifold is an algorithm that predicts a consensus structure for a set of aligned RNAs. This algorithm takes into consideration of both a thermodynamic energy model and sequence covariation. RNAalifold modifies the energy model by adding covariation score $\gamma(i,j)$ to evaluate the corresponding alignment columns i, j 's compensatory mutations.

$$\gamma(i,j) = \gamma'(i,j) + \delta \sum_{s \in S} \begin{cases} 0 & \text{if } (s_i, s_j) \text{ are pairable} \\ 0.25 & \text{if } s_i \wedge s_j \text{ are gaps} \\ 1 & \text{otherwise} \end{cases} \quad (1)$$

where S is the set of aligned sequences and γ' is used to evaluate covariance bonuses and penalties, δ is set to be 1 in RNAalifold.

There are two versions of RNAalifold: version 2002 [15] and version 2008 [4]. The major differences between the two versions are:

1. The old version uses a simplistic way to treat alignment gaps. Gaps within unpaired regions are ignored, which distorts the energy calculation. The new version fixes the problem by mapping the alignment indices back to the original positions for each sequence.
2. The old version calculates γ' based on simple qualitative arguments only. The new version uses trained new scoring matrices, named RIBOSUM.

We followed the new version of RNAalifold and developed LinearAlifold, which scales linearly with both the sequence length and the number of aligned sequences.

SARS-CoV-2 and SARS-related Datasets

We prepared a dataset to draw a representative sample of the most diverse SARS-CoV-2 and SARS-related genomes. Based on the genomes downloaded from GISAID [13] (downloaded on 4 April 2022) and NCBI ⁵ (genomes submitted from 1998 to 2019), we firstly filtered out low-quality genomes (i.e., genomes include unknown characters or are shorter than 28,000*nt*). After preprocessing, we get two datasets that contain about 40,000 SARS-CoV-2 (including Alpha, Beta, Delta, and Omicron variants) and 600 SARS-related genomes, respectively. Following LinearTurboFold, we prepared a greedy sampling algorithm to firstly selected 0.6 k most diverse genomes from the SARS-CoV-2 dataset, then to selected 0.4 k most diverse genomes from the SARS-related dataset. The general idea of the greedy sampling algorithm is to select genomes one by one with the highest number of mutation sites compared with the selected genomes.

Hybrid Reference Structure Construction in the 5' and 3' UTR regions of SARS-CoV-2

To get the hybrid reference structure in the UTR regions, we combined the experimentally guided structures from Huston et al. [18] and the experimentally determined end-to-end pairs (Arch3, ranges from (60,29868) to (80,29847)) from Ziv et al. [33, Fig.3] by the following steps:

1. Get the structures in 5' and 3' UTR regions from Huston et al. [18] (The UTRs range from 1 to 400 in the 5' UTR and from 29543 to 29876 in the 3' UTR).
2. Remove pair (i, j) from the structures if i or j is in the Arch3 region (SL3 from Huston et al. [18, Fig.2] is removed).
3. Combine the modified structures and the Arch3.

Software and Computing Environment

We use the following software:

⁵www.ncbi.nlm.nih.gov

- RNAalifold (Vienna RNAfold 2.4.16)
<https://www.tbi.univie.ac.at/RNA/>
- MAFFT 7.490
<https://mafft.cbrc.jp/alignment/software/>

We benchmarked RNAalifold and LinearAlifold on a Linux machine with 2 Intel Xeon E5-2660 v3 CPUs (2.60 GHz) and 377 GB memory, and used gcc (Ubuntu 9.3.0-17ubuntu1 20.04) to compile.

Code and Data Availability

Our code and data are released on GitHub:
github.com/LinearFold/LinearAlifold

Conflict of Interest

The authors declare no conflict of interest.

Author Contributions

L.H. conceived the idea and directed the project. L.Z. designed the main algorithm, implemented it, and evaluated it. S.L. contributed to the evaluations on both the RNAStralign dataset and SARS-CoV-2, as well as the comparison to LinearTurboFold. H.Z. contributed to the algorithm design. D.H.M. guided the evaluations on both the RNAStralign dataset and SARS-CoV-2. L.Z., L.H., S.L., H.Z., and D.H.M. wrote the manuscript.

Acknowledgments

This work was supported in part by National Institutes of Health Grant R01GM132185 (to D.H.M.) and National Science Foundation Grants IIS-1817231 and IIS-2009071 (to L.H.).

Supplementary Figures and Tables

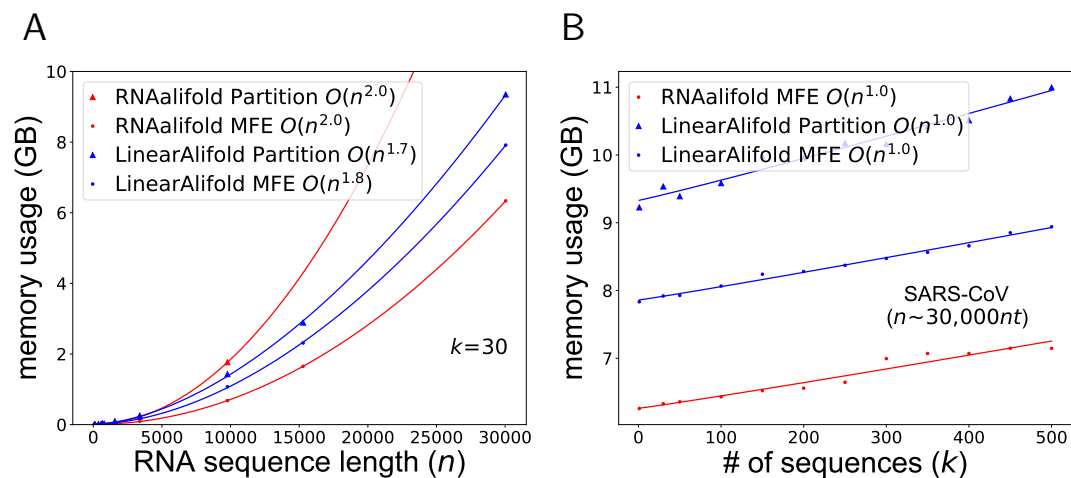


Figure S1: Memory usage comparisons between RNAalifold and LinearAlifold ($b = 100$). **A**: Memory usage comparison against sequence length (n) on multiple sequence alignments (MSA) ($k = 30$). **B**: Memory usage comparison against number of aligned sequences (k) on MSAs consisting SARS-CoV-2 and SARS-related genomes ($\sim 30,000nt$).

Region	Start	End	Length	Sequence	Gene	Accessibility	Conservation (# Mut. Sites)		
							SARS-CoV-2	SARS-related	GC %
Region 1	4027	4041	15	ACUUUAAUUGACAU	nsp3	0.60	0	8	20
Region 2	4028	4042	15	CUUUAAUUGACAUU	nsp3	0.60	0	8	20
Region 3	4028	4043	16	CUUUAAUUGACAUUA	nsp3	0.60	0	8	19
Region 4	4029	4043	15	UUUAAUUGACAUUA	nsp3	0.63	0	7	13
Region 5	4029	4044	16	UUUAAUUGACAUUAA	nsp3	0.63	0	8	13
Region 6	4030	4044	15	UUUAAUUGACAUUA	nsp3	0.63	0	8	13
Region 7	4031	4045	15	UAUAAUUGACAUUAAU	nsp3	0.63	0	8	13
Region 8	11564	11578	15	CCUAAUUUUUCUCAUA	nsp6	1.00	2	7	27
Region 9	14171	14185	15	UAUUAAACCUUGACCA	nsp12	1.00	0	8	33
Region 10	23593	23607	15	GACUAAUUCUCUCG	Spike	1.00	3	8	47
Region 11	23593	23608	16	GACUAAUUCUCUCGG	Spike	1.00	3	8	50
Region 12	23593	23609	17	GACUAAUUCUCUCGGC	Spike	1.00	3	8	53
Region 13	23593	23610	18	GACUAAUUCUCUCGGCG	Spike	0.99	3	8	56
Region 14	23593	23611	19	GACUAAUUCUCUCGGCGG	Spike	0.71	3	8	58
Region 15	23593	23612	20	GACUAAUUCUCUCGGCGGG	Spike	0.60	3	8	60
Region 16	23594	23608	15	ACUAAUUCUCUCGG	Spike	1.00	2	7	47
Region 17	23594	23609	16	ACUAAUUCUCUCGGC	Spike	1.00	2	7	50
Region 18	23594	23610	17	ACUAAUUCUCUCGGCG	Spike	0.99	2	7	53
Region 19	23594	23611	18	ACUAAUUCUCUCGGCGG	Spike	0.71	2	7	56
Region 20	23594	23612	19	ACUAAUUCUCUCGGCGGG	Spike	0.60	2	7	58
Region 21	23594	23613	20	ACUAAUUCUCUCGGCGGGC	Spike	0.60	2	8	60
Region 22	23595	23609	15	CUAAUUCUCUCGGC	Spike	1.00	2	6	53
Region 23	23595	23610	16	CUAAUUCUCUCGGCG	Spike	0.99	2	6	56
Region 24	23595	23611	17	CUAAUUCUCUCGGCGG	Spike	0.71	2	6	59
Region 25	23595	23612	18	CUAAUUCUCUCGGCGGG	Spike	0.60	2	6	61
Region 26	23595	23613	19	CUAAUUCUCUCGGCGGGC	Spike	0.60	2	7	63
Region 27	23596	23610	15	UAAUUCUCUCGGCG	Spike	0.99	2	5	53
Region 28	23596	23611	16	UAAUUCUCUCGGCGG	Spike	0.71	2	5	56
Region 29	23596	23612	17	UAAUUCUCUCGGCGGG	Spike	0.60	2	5	59
Region 30	23596	23613	18	UAAUUCUCUCGGCGGGC	Spike	0.60	2	6	61
Region 31	23597	23611	15	AAUUCUCUCGGCGG	Spike	0.71	2	4	60
Region 32	23597	23612	16	AAUUCUCUCGGCGGG	Spike	0.60	2	4	63
Region 33	23597	23613	17	AAUUCUCUCGGCGGGC	Spike	0.60	2	5	65
Region 34	23598	23612	15	AUUCUCUCGGCGGG	Spike	0.60	2	3	67
Region 35	23598	23613	16	AUUCUCUCGGCGGGC	Spike	0.60	2	4	69
Region 36	23599	23613	15	UUCUCUCUCGGCGGGC	Spike	0.60	2	3	73
Region 37	26619	26633	15	UGUCUUUCUACAAUUU	M	0.51	0	8	27
Region 38	29074	29088	15	AUACAAUGUAAACACA	N	0.68	2	6	27
Region 39	29074	29089	16	AUACAAUGUAAACAAA	N	0.68	2	6	25
Region 40	29075	29089	15	UACAAUGUAAACAAA	N	0.68	2	5	27

Figure S2: Accessible and conserved regions of SARS-CoV-2. 300 SARS-CoV-2 and 200 SARS-related genomes are included. MAFFT (-auto) are used to generate the MSA. Two constraints: 1) at most three mutated sites on SARS-CoV-2 genomes; 2) at least 50% samples are accessible in the region.

References

- [1] Omar O Abudayyeh, Jonathan S Gootenberg, Patrick Essletzbichler, Shuo Han, Julia Joung, Joseph J Belanto, Vanessa Verdine, David BT Cox, Max J Kellner, Aviv Regev, et al. RNA targeting with CRISPR-Cas13. *Nature*, 550(7675):280–284, 2017.
- [2] Nima Aghaepour and Holger H Hoos. Ensemble-based prediction of RNA secondary structures. *BMC Bioinformatics*, 14(139).
- [3] Jean Pierre Bachellerie, Jérôme Cavallé, and Alexander Hüttenhofer. The expanding snoRNA world. *Biochimie*, 84(8):775–790, 2002.
- [4] Stephan H Bernhart, Ivo L Hofacker, Sebastian Will, Andreas R Gruber, and Peter F Stadler. RNAalifold: improved consensus structure prediction for RNA alignments. *BMC Bioinformatics*, 9(1):1–13, 2008.
- [5] Edwin A Brown, Hangchun Zhang, Li-Hua Ping, and Stanley M Lemon. Secondary structure of the 5' nontranslated regions of hepatitis C virus and pestivirus genomic RNAs. *Nucleic Acids Research*, 20(19):5041–5045, 1992.
- [6] Stephen A Bustin and Tania Nolan. Pitfalls of quantitative real-time reverse-transcription polymerase chain reaction. *Journal of Biomolecular Techniques: JBT*, 15(3):155, 2004.
- [7] Jamie J Cannone, Sankar Subramanian, Murray N Schnare, James R Collett, Lisa M D'Souza, Yushi Du, Brian Feng, Nan Lin, Lakshmi V Madabusi, Kirsten M Müller, Nupur Pande, Zhidi Shang, Nan Yu, and Robin R Gutell. The comparative RNA web (crw) site: An online database of comparative sequence and structure information for ribosomal, intron, and other RNAs. *BioMed Central Bioinformatics*, 3(2), 2002.
- [8] Peter Clote, Yann Ponty, and Jean-Marc Steyaert. Expected distance between terminal nucleotides of RNA secondary structures. *Journal of mathematical biology*, 65(3):581–599, 2012.
- [9] Ye Ding and Charles E Lawrence. A statistical sampling algorithm for RNA secondary structure prediction. *Nucleic acids research*, 31(24):7280–7301, 2003.
- [10] Chuong Do, Daniel Woods, and Serafim Batzoglou. CONTRAfold: RNA secondary structure prediction without physics-based models. *Bioinformatics*, 22(14):e90–e98, 2006.
- [11] Jennifer A. Doudna and Thomas R. Cech. The chemical repertoire of natural ribozymes. *Nature*, 418(6894):222–228, 2002.
- [12] S. R. Eddy. Non-coding RNA genes and the modern rna world. *Nature Reviews Genetics*, 2(12):919–929, 2001.
- [13] Stefan Elbe and Gemma Buckland-Merrett. Data, disease and diplomacy: GISAID's innovative contribution to global health. *Global challenges*, 1(1):33–46, 2017.
- [14] Hafeez S Haniff, Yuquan Tong, Xiaohui Liu, Jonathan L Chen, Blessy M Suresh, Ryan J Andrews, Jake M Peterson, Collin A O'Leary, Raphael I Benhamou, Walter N Moss, et al. Targeting the SARS-CoV-2 RNA genome with small molecule binders and ribonuclease targeting chimera (RIBOTAC) degraders. *ACS Central Science*, 6(10):1713–1721, 2020.
- [15] Ivo L Hofacker, Martin Fekete, and Peter F Stadler. Secondary structure prediction for aligned RNA sequences. *Journal of Molecular Biology*, 319(5):1059–1066, 2002.
- [16] Liang Huang and David Chiang. Better k-best parsing. *Proceedings of the Ninth International Workshop on Parsing Technologies*, pages 53–64, 2005.
- [17] Liang Huang, He Zhang, Dezhong Deng, Kai Zhao, Kaibo Liu, David A Hendrix, and David H Mathews. LinearFold: linear-time approximate RNA folding by 5'-to-3' dynamic programming and beam search. *Bioinformatics*, 35(14):i295–i304, 07 2019. ISSN 1367-4803. doi: 10.1093/bioinformatics/btz375. URL <https://doi.org/10.1093/bioinformatics/btz375>.
- [18] Nicholas C Huston, Han Wan, Madison S Strine, Rafael de Cesaris Araujo Tavares, Craig B Wilen, and Anna Marie Pyle. Comprehensive in vivo secondary structure of the SARS-CoV-2 genome reveals novel regulatory motifs and mechanisms. *Molecular Cell*, 81(3):584–598, 2021.
- [19] Kazutaka Katoh and Daron M Standley. MAFFT multiple sequence alignment software version 7: improvements in performance and usability. *Molecular Biology and Evolution*, 30(4):772–780, 2013.
- [20] B. Knudsen and J. Hein. Pfold: RNA secondary structure prediction using stochastic context-free grammars. *Nucleic Acids Research*, 31(13):3423–3428, 2003.
- [21] Wan-Jung C Lai, Mohammad Kayedkhordeh, Erica V Cornell, Elie Farah, Stanislav Bellaousov, Robert Rietmeijer, David H Mathews, and Dmitri N Ermolenko. mRNAs and lncRNAs intrinsically form secondary structures with short end-to-end distances. *Nature Communications*, 9(1):4328, 2018.
- [22] Sizhen Li, He Zhang, Liang Zhang, Kaibo Liu, Boxiang Liu, David H Mathews, and Liang Huang. LinearTurboFold: Linear-time global prediction of conserved structures for RNA homologs with applications to SARS-CoV-2. *Proceedings of the National Academy of Sciences*, 118(52), 2021.

- [23] Zhi John Lu and David H Mathews. Efficient siRNA selection using hybridization thermodynamics. *Nucleic Acids Research*, 36(2):640–647, 2008.
- [24] Zhi John Lu, Jason W Gloor, and David H Mathews. Improved RNA secondary structure prediction by maximizing expected pair accuracy. *RNA*, 15(10):1805–1813, 2009.
- [25] Eric P Nawrocki and Sean R Eddy. Infernal 1.1: 100-fold faster RNA homology searches. *Bioinformatics*, 29(22):2933–2935, 2013.
- [26] Justin Ritz, Joshua S Martin, and Alain Laederach. Evolutionary evidence for alternative structure in RNA sequence co-variation. *PLoS Computational Biology*, 9(7):e1003152, 2013.
- [27] Steffen Schubert, Arnold Grünweller, Volker A Erdmann, and Jens Kurreck. Local RNA target structure influences siRNA efficacy: systematic analysis of intentionally designed binding regions. *Journal of Molecular Biology*, 348(4):883–893, 2005.
- [28] Lei Sun, Pan Li, Xiaohui Ju, Jian Rao, Wenzhe Huang, Lili Ren, Shaojun Zhang, Tuanlin Xiong, Kui Xu, Xiaolin Zhou, et al. In vivo structural characterization of the SARS-CoV-2 RNA genome identifies host proteins vulnerable to repurposed drugs. *Cell*, 184(7):1865–1883, 2021.
- [29] Zhen Tan, Yinghan Fu, Gaurav Sharma, and David H Mathews. TurboFold II: RNA structural alignment and secondary structure prediction informed by multiple homologs. *Nucleic Acids Research*, 45(20):11570–11581, 2017.
- [30] He Zhang, Liang Zhang, Sizhen Li, David H Mathews, and Liang Huang. LinearSampling: Linear-time stochastic sampling of RNA secondary structure with applications to SARS-CoV-2. *BioRxiv*, 2020.
- [31] He Zhang, Liang Zhang, David H Mathews, and Liang Huang. LinearPartition: linear-time approximation of RNA folding partition function and base-pairing probabilities. *Bioinformatics*, 36(Supplement_1):i258–i267, 2020.
- [32] Liang Zhang, He Zhang, David H. Mathews, and Liang Huang. ThreshKnot: Thresholded ProbKnot for Improved RNA Secondary Structure Prediction. *bioRxiv*, 2019.
- [33] Omer Ziv, Jonathan Price, Lyudmila Shalamova, Tsveta Kamenova, Ian Goodfellow, Friedemann Weber, and Eric A Miska. The short-and long-range RNA-RNA interactome of SARS-CoV-2. *Molecular Cell*, 80(6):1067–1077, 2020.